LANGMUIR

pubs.acs.org/Langmuir Article

Pore-Scale Study on Shale Oil–CO_2–Water Miscibility, Competitive Adsorption, and Multiphase Flow Behaviors

Han Wang, Jianchao Cai,* Yuliang Su, Zhehui Jin,* Mingshan Zhang, Wendong Wang, and Guanqun Li

Cite This: *Langmuir* 2023, 39, 12226–12234 Read Online

ACCESS | Metrics & More | Article Recommendations

ABSTRACT: Due to the fracturing fluid imbibition and primary water, oil–water two-phase fluids generally exist in shale nanoporous media. The effects of water phase on shale oil recovery and geological carbon sequestration via CO_2 huff-n-puff is non-negligible. Meanwhile, oil–CO_2 miscibility after CO_2 huff-n-puff also has an important effect on oil–water two-phase flow behaviors. In this work, by considering the oil–CO_2 competitive adsorption behaviors and the effects of oil–CO_2 miscibility on water wettability, an improved multicomponent and multiphase lattice Boltzmann method is proposed to study the effects of water phase on CO_2 huff-n-puff. Additionally, the effects of oil–CO_2 miscibility on oil–water flow behaviors and relative permeability are also discussed. The results show that due to Jamin's effect of water droplets in oil-wetting pores and the capillary resistance of bridge-like water phase in water-wetting pores, CO_2 can hardly diffuse into the oil phase, causing a large amount of remaining oil. As water saturation increases, Jamin's effect and the capillary resistance become more pronounced, and the CO_2 storage mass gradually decreases. Then, based on the results from molecular dynamics simulations, the influences of oil–CO_2 miscibility on oil–water relative permeability in calcite nanoporous media are studied, and as the oil mass percentage in the oil–CO_2 miscible system decreases, the oil/water relative permeability decreases/increases. The improved lattice Boltzmann model can be readily extended to quantitatively calculate geological CO_2 storage mass considering water saturation and calculate the accurate oil–water relative permeability based on the real 3D digital core.

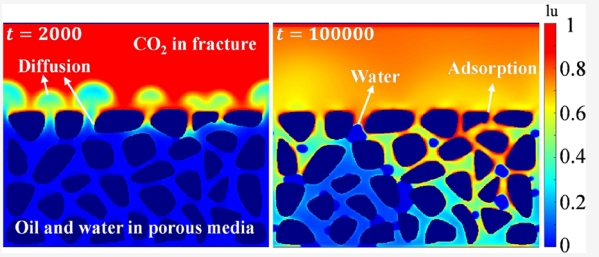

INTRODUCTION

Shale nanoporous media is originally saturated with water during the early stage of formation, and due to the water-wet inorganic mineral and specific pore structures, some connate water remains in pores during oil migration.[1,2] In addition, shale oil production mainly relies on hydraulic fracturing,[3−5] resulting in fracturing fluids encroaching into pores through spontaneous and/or forced imbibition.[6−8,9,10,11,12] Hence, oil–water two-phase fluids generally exist in shale nanoporous media.[13−15] CO_2 huff-n-puff is not only an effective way to enhance shale oil recovery[16−18] but also a potential means of geologically sequestrating CO_2.[19,20] CO_2 diffusion, oil–CO_2 competitive adsorption, and oil–CO_2–water miscible/immiscible flow behaviors are the most important microscopic mechanisms in CO_2 huff-n-puff,[21−23,24] which are inevitably influenced by the presence of the water phase. Meanwhile, oil–CO_2 miscibility after CO_2 huff-n-puff also has an important effect on oil–water two-phase flow behaviors. Therefore, it is imperative to investigate the effects of water phase on CO_2 huff-n-puff and the effects of oil–CO_2 miscibility on oil–water relative permeability.

Depending on rock wettability, water saturation, and pore size and structures, water phase exists in porous media in various distinct forms, including film, droplet, bridge, cluster, and so forth,[2,25−27] and eventually affects the fluid physical behavior by capillary force and interface action.[28] In recent years, some scholars have studied the influence of the water phase on CO_2-enhanced shale oil/gas recovery from microscopic perspectives by using molecular dynamics (MD) simulations. Liu et al.[29] used MD simulations to study supercritical CO_2 breaking through a water bridge and how it enhances oil recovery in quartz nanopores. However, the breakthrough of the water bridge depends on the continuous injection pressure and water bridge thickness which are strongly dependent on water saturation and surface wettability.[26] As the well is shut in after CO_2 injection, whether the water bridge can be broken in shale porous media under different water saturations is still under debate. Meanwhile, Luan et al.[30] studied the effect of water film rupture on oil displacement in dead-end nanopores by supercritical CO_2. They found that the water film rupture time is greatly influenced by its thickness, CO_2 injection pressure, and pore

Received: June 9, 2023
Revised: August 3, 2023
Published: August 15, 2023

depth. The injected CO_2 can also influence oil and water wettability and ultimately affect oil−water relative permeability. Yong et al.[31] simulated nanoscopic water droplets on a graphite substrate and showed that the water contact angle increases as the CO_2 content increases. Zhou et al.[32] studied the effect of CO_2 pressure on the CO_2−water−kerogen contact angle and found that with the increase of CO_2 pressure, the water contact angle weakly increases. Most of the current MD studies are conducted based on the single-pore model,[33] while the collective effect of multiple water-phase occurrence states in porous media on CO_2 diffusion, competitive adsorption, and oil-phase relative permeability has not been fully taken into account. In addition to MD simulations, some scholars studied the influence of water phase on CO_2 huff-n-puff by experimental measurements. Li et al.[34] investigated the effect of water on CO_2 huff-n-puff EOR performance. They reported that the oil recovery declines by ∼45% after seven huff-n-puff cycles compared to that without water. Experimental studies have difficulties in terms of quantitatively or qualitatively analyzing the effect of various parameters (such as wettability, competitive adsorption capacity, water saturation, etc.) from microscopic perspectives, and they are usually time-consuming due to the ultralow permeability of shale rocks.

In this regard, pore-scale simulation can be an effective tool to explore the influences of water phase on CO_2 huff-n-puff by taking into account the complex water distributions in porous media and various parameters from microscopic perspectives. Lattice Boltzmann method (LBM) is an effective pore-scale simulation method to simulate physical and chemical behaviors.[35−373839] Wei et al.[40] performed the immiscible three-phase Shan−Chen LBM to investigate the effect of droplet shape and size, gravity, and meniscus curvature on the spontaneous motion of droplets and bubbles.[40] Based on a color-gradient LBM, Zhu et al.[41] studied the effects of wettability, viscosity ratio, and capillary number on the relative permeability. Li et al.[42] and Yu et al.[43] modeled an immiscible three-phase flow and investigated the effect of surface wettability and inlet average velocity on the droplet dynamic behaviors and fluid distributions. Tang et al.[44] proposed an improved oil−CO_2−water three-phase LBM based on the Shan−Chen multiple relaxation time type and discussed the displacement behaviors of CO_2 with different injection conditions. However, these studies are all limited to the conventional pore scale and immiscible three-phase fluid flows. Currently, there are some studies on the CO_2−water−solid chemical reactions by LBM which involves CO_2 diffusion and CO_2−water immiscible flow.[45−4748] Nevertheless, they are not suitable for the investigations on the effects of water phase on CO_2 huff-n-puff, considering the diffusion and miscible behaviors. Recently, we proposed a pore-scale pseudopotential LBM to simulate oil−CO_2 diffusion, competitive adsorption, and miscible flow behaviors to investigate the CO_2 huff-n-puff and discuss the oil−CO_2 flow capacity.[49] However, the water phase was not considered in the model, which is non-negligible.

Therefore, in this work, an improved oil−CO_2−water multicomponent and multiphase LBM (MCMP-LBM) is first proposed, and the CO_2 diffusion, oil−CO_2 competitive adsorption behaviors, and the effect of oil−CO_2 miscibility on the water contact angle are considered. Then, the interfacial tension and the effects of oil−CO_2 miscibility on water wettability are verified. Based on the model, the effects of water phase on CO_2 huff-n-puff and CO_2 sequestration are investigated. Finally, the effects of oil−CO_2 miscibility on oil−water flow behaviors and relative permeability are discussed. Based on the parameters obtained by fitting the MD simulation results, the enhancement on oil−water relative permeability due to CO_2 is studied.

Oil−CO_2−Water Multicomponent and Multiphase Lattice Boltzmann Method. An improved LBM based on modified oil−CO_2−water interaction forces is proposed to capture the oil−CO_2−water diffusion, competitive adsorption, and multiphase flow behaviors. The LBM fundamental governing equations of oil−CO_2−water and oil−CO_2 are the same, which can be found in our previous work.[49] Compared with the oil−CO_2 system, the innovation of this model lies in the treatment of three-phase interaction forces, which are the fluid−fluid interaction force ($\mathbf{F}_{\sigma,\mathrm{int}}$), fluid−surface interaction force ($\mathbf{F}_{\sigma,\mathrm{ads}}$), and body force ($\mathbf{F}_{\sigma,\mathrm{b}} = (F_{\sigma,\mathrm{b},x}, F_{\sigma,\mathrm{b},y})$).

To capture diffusion and interfacial tension, $\mathbf{F}_{\sigma,\mathrm{int}}$ can be expressed by

$$\begin{aligned}\mathbf{F}_{\sigma_1,\mathrm{int}}(\boldsymbol{x},t) = -\psi_{\sigma_1}(\boldsymbol{x})[&G_{\sigma_1\sigma_1}\sum_{\alpha} w(|\mathbf{e}_\alpha|^2)\psi_{\sigma_1}(\boldsymbol{x}+\mathbf{e}_\alpha\delta_t)\mathbf{e}_\alpha \\ &+ G_{\sigma_1\sigma_2}\sum_{\alpha} w(|\mathbf{e}_\alpha|^2)\psi_{\sigma_2}(\boldsymbol{x}+\mathbf{e}_\alpha\delta_t)\mathbf{e}_\alpha \\ &+ G_{\sigma_1\sigma_3}\sum_{\alpha} w(|\mathbf{e}_\alpha|^2)\psi_{\sigma_3}(\boldsymbol{x}+\mathbf{e}_\alpha\delta_t)\mathbf{e}_\alpha]\end{aligned} \tag{1}$$

where $G_{\sigma_1\sigma_1}$ is an interaction parameter of the same fluid; $G_{\sigma_1\sigma_2}$ and $G_{\sigma_1\sigma_3}$ are the parameters of the fluid−fluid cohesion force controlling the phases separation and miscibility; $\psi_{\sigma_1} = 1 - \exp(-\rho_{\sigma_1})$ is a pseudopotential; and ρ_{σ_1} is the density with $\rho_{\sigma_1} = \sum_\alpha f_{\sigma_1,\alpha}$.

To capture the wettability, $\mathbf{F}_{\sigma,\mathrm{ads}}$ can be expressed as

$$\mathbf{F}_{\sigma_1,\mathrm{ads}}(\mathbf{x},t) = -G_{\sigma_1 s}\psi_\sigma(\mathbf{x},t)\sum_{\alpha} w(|\mathbf{e}_\alpha|^2)s(\mathbf{x}+\mathbf{e}_\alpha\delta_t)\mathbf{e}_\alpha \tag{2}$$

where $G_{\sigma_1 s}$ is a fluid−solid interaction parameter. In this work, there are a few assumptions for the adsorption of oil−CO_2−water on the pore surface in lattice Boltzmann (LB) simulations: (1) Compared to the competitive adsorption of oil and CO_2, the competitive adsorption of CO_2 and water on the wall can be ignored. It is because the solubility of CO_2 in water is very small compared to that in oil phase. (2) The nanoconfined flow behaviors due to the water−surface interaction can be accurately characterized by the difference in the lattice viscosity between the near-wall and bulk water phase. (3) The competitive adsorption of oil−CO_2 phase can be characterized by tuning the adsorption capacity of CO_2−surface while keeping the oil−surface adsorption constant. Eq 2 is adopted for oil phase and water phase in our simulations, which can not only characterize the oil−water−surface three-phase contact angle but also ensure the constant adsorption capacity of the oil phase on the surface . To capture the heterogeneous CO_2 density distribution, the CO_2−surface interaction force ($\mathbf{F}_{\sigma,\mathrm{ads}}$) coupling an exponential formula is adopted[50,51]

$$\mathbf{F}_{\mathrm{cs,ads}}(\mathbf{x},t) = -G_{\mathrm{cs}}\psi(\mathbf{x},t)\sum_{\alpha} \mathrm{e}^{-|\mathbf{x}_\alpha|/\lambda}\mathbf{e}_\alpha \tag{3}$$

https://doi.org/10.1021/acs.langmuir.3c01570
Langmuir 2023, 39, 12226−12234

where G_{cs} is a CO_2−surface interaction parameter; $\mathbf{x}_{\alpha}$ is the distance from the solid surface in direction $\boldsymbol{\alpha}$, and when there is no solid surface in direction $\boldsymbol{\alpha}$, $\mathbf{x}_{\alpha} = 0$; $\lambda = 0.35$ nm[49] is a constant affecting the thickness of the near-surface region.[52]

Model Verification. In order to verify the proposed model, the Laplace test and contact angle calculation are conducted. The verification of diffusion, adsorption, and flow behaviors can be found in our previous works.[49] First, the Laplace test is conducted, and the capillary number is calculated to verify the interfacial properties in simulation. Then, the oil−water−surface contact angle calculation and the effects of CO_2 on the water contact angle in LB simulations are verified and studied.

Laplace Test. In our simulation, CO_2−oil interfacial tension is not considered, as CO_2 and oil can be miscible. Thus, only oil−water and CO_2−water interfacial tensions are considered. The CO_2−water interfacial tension is generally 30 mN/m at typical reservoir conditions (343 K and 20 MPa),[53−55]57 while that of oil−water is generally 44 mN/m.[58−60]62,63 As the CO_2 mole fraction in the oil phase increases, the CO_2/oil−water interfacial tension approaches to that of CO_2−water.[64] In LB simulations, it is difficult to adjust interfacial tension independently from the diffusion, adsorption, and surface wettability. Therefore, in this work, the oil−water and CO_2−water interfacial tensions are assumed roughly equal. During the Laplace test, a square water phase in the oil phase and CO_2 phase is placed, respectively. Then, the water phase gradually becomes a spherical droplet with the fluid−fluid interaction force $G_{wo} = 2.1$, $G_{wc} = 2.1$, and $G_{co} = 1$, and unless otherwise specified, the above fluid−fluid interaction parameters are used in the following simulations. The internal and external pressure differences (p_{in} and p_{out}) of the droplet can be obtained by the pressure calculation formula,[65,66] as shown in eq 4. The linear relationship between the pressure difference and the reciprocal of the droplet radius with the lattice IFT ≈ 0.065 is shown in Figure 1, which is in accordance with the Laplace law, as shown in eq 5.

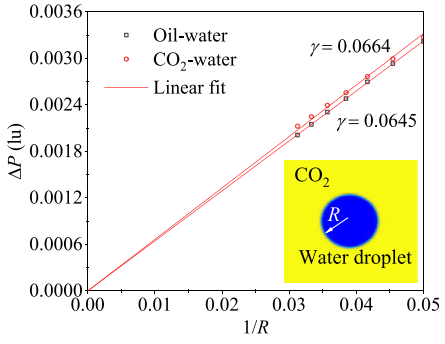

Figure 1. Relationship between the pressure difference of the droplet and the reciprocal of the droplet radius in the Laplace test.

The capillary number, Ca, is defined as the ratio of the external force $F_{b,x}$ in the flow direction (i.e., x-direction) to the lattice IFT, γ, in LB simulations,[67] $Ca = F_{b,x}/\gamma$. Ca represents the relative importance of viscous force ($u\mu$) over the capillary force (γ). The oil/CO_2−water flows can be driven by an external force $F_{b,x}$ ranging from 2×10^{-4} to 2×10^{-6}, while the capillary number $Ca = F_{b,x}/\gamma$ ranges from 3.1×10^{-3} to 3.1×10^{-5}, which is within the typical range of capillary numbers in porous media.[68]

$$p = c_s^2 \sum_{i=1}^{3} \rho_{\sigma_i} + c_s^2 \sum_{i=1}^{3} \sum_{j \neq i} G_{\sigma_i \sigma_j} \psi_{\sigma_i} \psi_{\sigma_j} \tag{4}$$

$$\gamma = (p_{in} - p_{out})R \tag{5}$$

Wettability. As shown in eq 2, the fluid−surface interaction force, $G_{\sigma_i s}$, can be tuned to obtain different oil−water contact angle values, and $G_{ws} = -G_{os}$. As shown in Figure 2A, the water phase forms a droplet on a solid surface due to the oil−surface, water−surface, and oil−water interactions. The oil−water−surface contact angle values can be calculated according to the droplet width and height. With an increasing water−surface interaction parameter G_{ws}, the oil−water−surface contact angle increases. In the process of CO_2 huff-n-puff, CO_2 diffuses into the oil phase, which can alter the CO_2/oil−water−surface contact angle. As the CO_2 pressure increases, CO_2/oil−water−surface contact angle gradually increases due to the strong surface adsorption capacity of CO_2.[31,69,70] The effect of CO_2 on CO_2/oil−water−surface contact angle is shown in Figures 2B and 3. In addition, as the CO_2−surface interaction parameter G_{cs} decreases, the CO_2 adsorption capacity on the solid surface increases, which increases the CO_2/oil−water−surface contact angle.

RESULTS AND DISCUSSION

Based on the SEM image, a conceptual model of fractures and porous media is constructed to simulate CO_2 huff-n-puff, as shown in Figure 4.

In this section, the CO_2 huff-n-puff process with water saturation $S_w = 0.2$ based on the conceptual model is studied. For water-wetting and oil-wetting porous media, $G_{ws} = -G_{os} = -1$ and $G_{ws} = -G_{os} = 1$, respectively, and the corresponding contact angles of water at $X_{CO_2} = 0$ are equal to 44.2 and 159.5°. Additionally, $G_{cs} = -0.025$. Then, the specific simulation methods and steps are as follows. First, the water phase is randomly distributed in 20% of total grids in porous media, while the rest are filled by oil phase. Then, the oil−water phase flow in porous media is driven by an external body force $F_{b,x} = 0.002$ (to ensure that the water phase droplets can be randomly distributed in the porous media). Due to the oil−water interfacial force, the water phase gradually gathers and distributes randomly in the porous media, as shown in Figure 5.

As shown in Figure 5, as time t increases, CO_2 gradually diffuses into, and oil is displaced out from, the porous medium. Additionally, small amounts of water droplets in oil-wetting pores overcome Jamin's effect and are displaced out from the porous media. As shown in Figure 6, due to Jamin's effect of water droplets in oil-wetting pores and the capillary resistance of bridge-like water phase in water-wetting pores, CO_2 cannot diffuse into the oil phase, causing a large amount of oil confined in porous media. Figure 7 shows the lattice storage mass of CO_2 in porous media versus time. As t increases, the storage mass of CO_2 increases.

Effects of CO_2−Surface Molecular Interactions. Shale matrix contains organic matter (kerogen) and inorganic matter (quartz, feldspar, calcite, etc.), resulting in diverse CO_2 adsorption capacities in various porous media. Therefore, in this subsection, the effects of different CO_2 adsorption capacities on CO_2 storage amount in oil-wetting and water-wetting porous media under low water saturation conditions are discussed. $G_{cs} = 0$, $G_{cs} = -0.025$, and $G_{cs} = -0.05$ are used

https://doi.org/10.1021/acs.langmuir.3c01570
Langmuir 2023, 39, 12226−12234

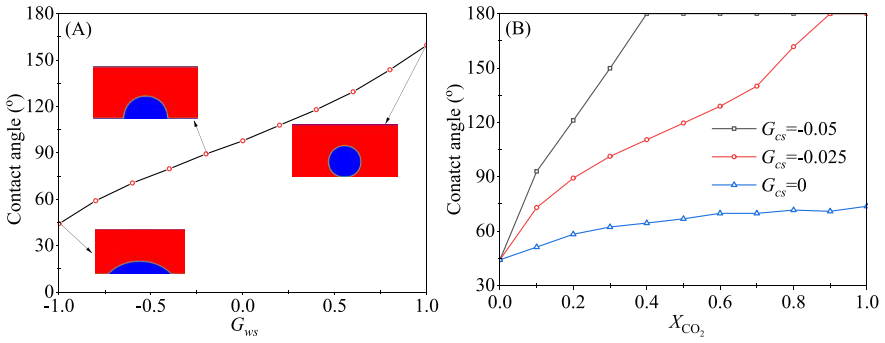

Figure 2. CO_2/oil−water−surface contact angle vs G_{ws}, G_{cs}, and CO_2 mass content X_{CO_2} in the oil phase. (A) G_{ws}, (B) G_{cs} and X_{CO_2}, $G_{ws} = -G_{os} = -1$.

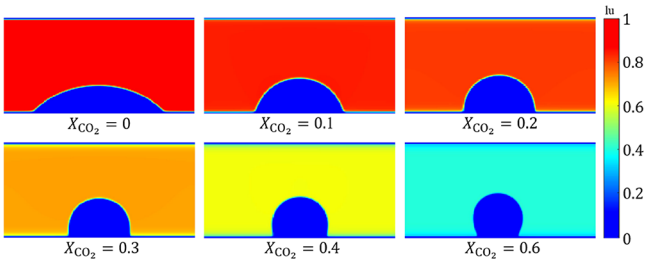

Figure 3. Oil density distributions at different CO_2 mass contents in the oil phase, and $G_{cs} = -0.025$.

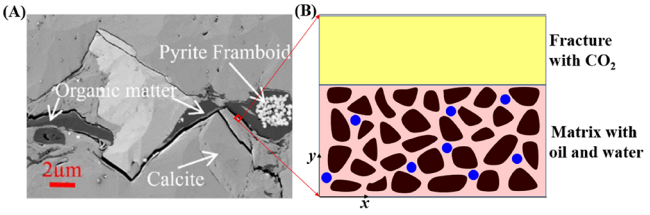

Figure 4. SEM image (A) and conceptual model of fractures and porous media (B). Black: solid matrix; yellow phase: CO_2; red phase: oil; and blue phase: water. Left and right boundaries: periodic conditions.

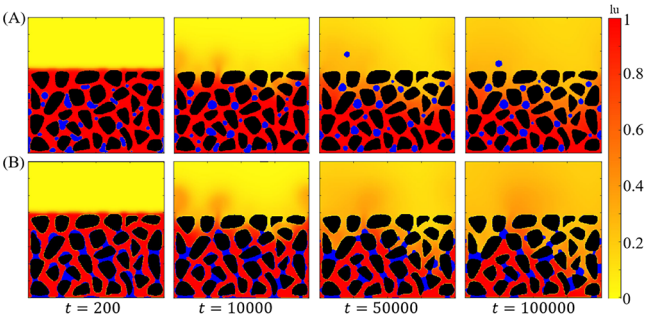

Figure 5. Oil−CO_2−water distributions vs time. (A) Oil-wetting porous media; (B) water-wetting porous media. Yellow phase: CO_2; red phase: oil; blue phase: water; and black phase: rock.

to characterize different CO_2 adsorption capacities. As G_{cs} decreases, CO_2 adsorption capacity increases.

Figure 8 presents the CO_2 storage mass versus t and G_{cs} in oil-wetting and water-wetting porous media, and Figure 9 shows the CO_2 density distributions at lattice t = 100,000. With a decrease of G_{cs} (an increase of CO_2 adsorption capacity), the near-wall CO_2 adsorption density increases.

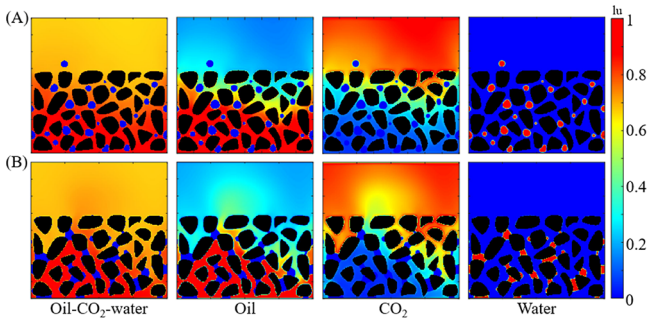

Figure 6. Oil, CO_2, and water distributions in porous media, with t = 100,000. (A) Oil-wetting porous media and (B) water-wetting porous media.

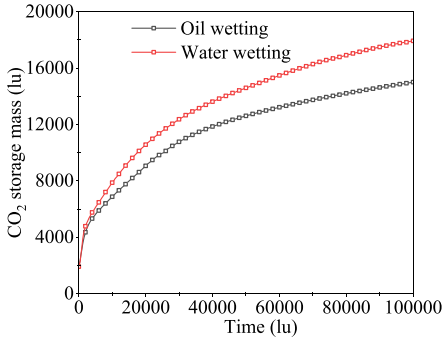

Figure 7. CO_2 storage mass vs time.

Then, CO_2 easily diffuses into the oil phase along the pore wall, and the CO_2 mass in porous media increases gradually. In the water-wetting porous media, the water contact angle in the oil−CO_2 miscible phase increases, and as $G_{cs} = -0.05$ and CO_2 density increases, water attached to the surface gradually detaches from the wall and forms droplets. In the process of CO_2 diffusion, the water droplets in the porous media can be displaced and flow in pore-throat structures, and under certain conditions (depending on the pore structure, the initial distribution of the water phase, etc.), the water droplets can also be displaced out of the porous media.

Effects of Water Saturation. In this subsection, the effect of different water saturations (S_w = 0, 0.1, 0.2, 0.3, and 0.4) on CO_2 storage is investigated with five random water-phase distributions used for each S_w case. The representative oil−CO_2−water distributions for each S_w case are shown in Figure 10. As S_w increases, the number and volume of droplets in the pore throat of oil-wetting pores increase, which makes it

https://doi.org/10.1021/acs.langmuir.3c01570
Langmuir 2023, 39, 12226−12234

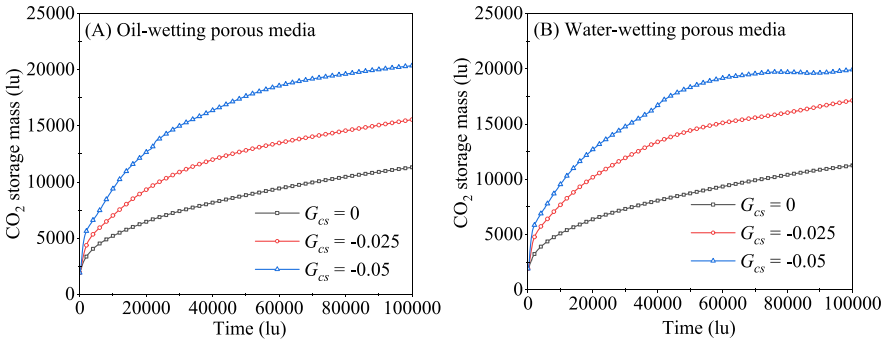

Figure 8. CO_2 storage mass in oil-wetting and water-wetting porous media vs t and G_{cs}. (A) Oil-wetting porous media and (B) water-wetting porous media.

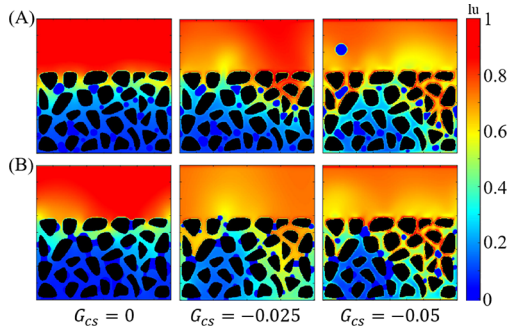

Figure 9. CO_2 density distributions with different G_{cs}: (A) Oil-wetting porous media and (B) water-wetting porous media.

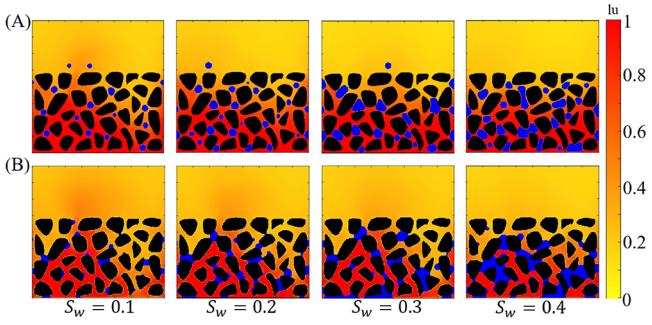

Figure 10. Oil−CO_2−water distribution vs water saturation S_w: (A) oil-wetting porous media, $G_{ws} = -G_{os} = 1$, and the contact angle of water is 159.5°; (B) water-wetting porous media, $G_{ws} = -G_{os} = -1$, and the contact angle of water is 44.2°. $G_{cs} = -0.025$.

difficult for CO_2 to diffuse into the depth of porous media. In the water-wetting porous media, the water phase gradually occupies the adjacent solid matrix and forms a bridge plug, completely blocking CO_2 diffusion. When $S_w = 0$, the evolution of CO_2 storage mass in oil-wetting porous media is shown, as in Figure 11A. Until t = 250,000, CO_2 diffusion does not reach equilibrium. Through the exponential function fitting of the mass−time curve, with $t = \infty$, the CO_2 storage mass after simulation equilibrium can be obtained. Figure 11B shows the relationship between CO_2 storage mass and S_w in oil-wetting and water-wetting porous media. As S_w increases, Jamin's effect of water droplets in oil-wetting pores and the capillary resistance of bridge-like water phase in water-wetting pores become more pronounced. In addition, water phase occupies more pore space in porous media, and the solubility of CO_2 in water is negligible compared to that in oil phase. As a result, CO_2 storage mass gradually decreases.

Effect of CO_2 on Oil Relative Permeability Enhancement. It is assumed that when CO_2 and oil are miscible, oil−CO_2−water in porous media becomes a three-component two-phase system. Based on the velocity and density distributions of oil (nC_8) and CO_2-miscible phase in calcite pores from MD simulations,[22] the CO_2/oil−water two-phase flow in calcite porous media is simulated, and the effect of CO_2 on the oil relative permeability enhancement is discussed.

The flow parameters of the water phase in porous media are fixed, independent of the oil mass percentage (OMP) in oil−CO_2 miscible phase. The bulk water viscosity $\mu_{w,bulk}$ equals 1 mP·s, while the near-wall water viscosity $\mu_{w,wall} = (-0.018\theta + 0.5)\mu_{w,bulk}$ can be obtained from the work of Wu et al.[71] The contact angle θ in the viscosity calculation is 44.1° for OMP = 100%, while it is independent of OMP. The zero-boundary slip velocity condition is adopted. The viscosity and boundary conditions can be realized by the lattice viscosity and the slip boundary combination parameter $r_w = 0$.[13]

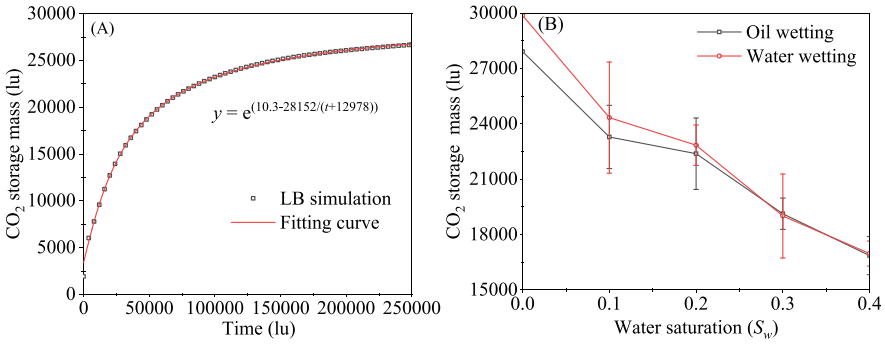

Figure 11. CO_2 storage mass versus t and S_w. (A) Lattice time t, (B) water saturation S_w, and t = 250,000.

https://doi.org/10.1021/acs.langmuir.3c01570
Langmuir 2023, 39, 12226−12234

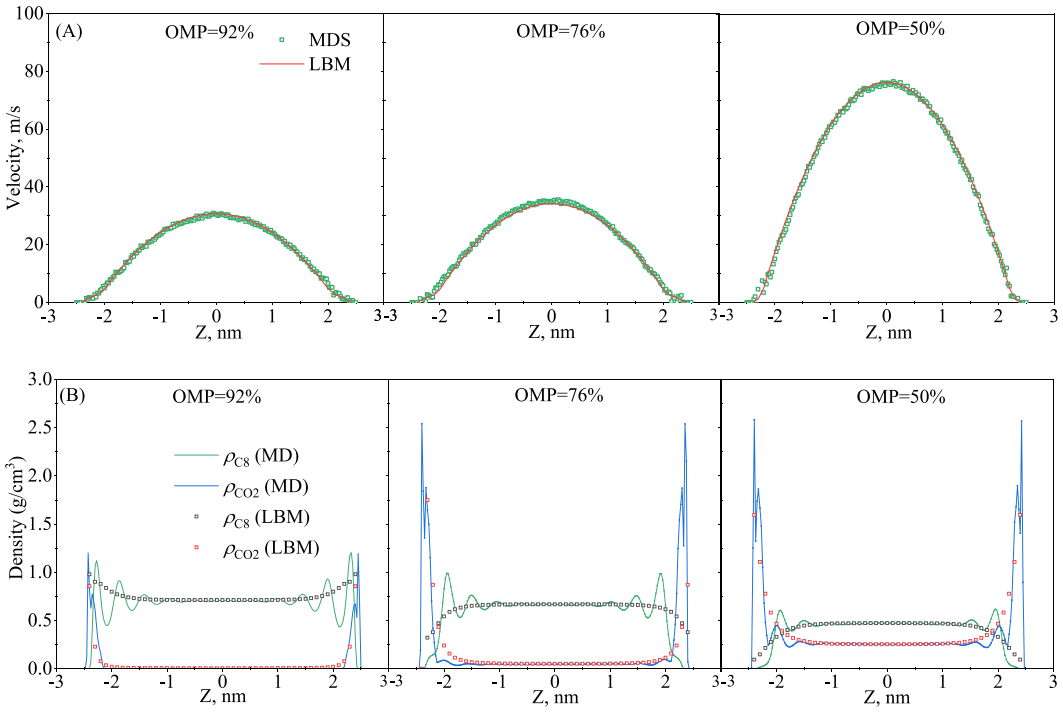

Figure 12. Velocity and density distribution of nC_8 and CO_2 from MD and LB simulations. (A) Velocity and (B) density.

The oil−CO_2 miscible phase flow parameters are difficult to obtain theoretically or experimentally. Therefore, these parameters are determined according to the miscible velocity and density distributions from the MD simulations by Zhang et al.[22] First, the external body force $F_{b,x}$, bulk oil−CO_2 miscible viscosity, near-wall oil−CO_2 miscible viscosity, and near-wall oil−CO_2 thickness are adjusted to fit the velocity distributions for OMP = 92% from MD simulations. After the fitting, these parameters can be used to simulate the oil/CO_2−water two-phase flow with OMP = 92%. Then, with fixed $F_{b,x}$, the bulk oil−CO_2 miscible viscosity, near-wall oil−CO_2 miscible viscosity, and near-wall oil−CO_2 thickness are adjusted to fit the velocity distribution, with OMP equaling 76 and 50%.

The relative permeability calculations are given in eqs 6 and 7. The pure oil-phase velocity is necessary to obtain the pure oil-phase relative permeability. However, in the simulation process, due to the competitive adsorption of CO_2 and oil phase, the oil phase density is highly heterogeneous, and its influence on the relative permeability cannot be ignored; therefore, the density distributions of oil phase in the oil−CO_2 miscible phase need to be determined. Based on the fitting of density distributions from MD simulations, the density distribution parameters of the oil−CO_2 miscible phase on the surface are obtained.[49] According to the equal-area principle (the specific fitting details can be found in our previous work[49]), by adjusting the oil−surface force parameter G_{os} and CO_2−surface force parameter G_{cs} in eq 3, the density fitting results are shown in Figure 12B. It is noted that G_{os} and G_{cs} in density fitting are only used for the calculation of relative permeability, and these are indicated in Table 1.

In our flow simulations, $G_{cs} = -0.05$ is used to characterize the adsorption behaviors and the effect of CO_2 phase on water contact angles. With $G_{ws} = -G_{os} = -1$, the contact angle can be determined by Figure 2B. For OMP = 100%, the water contact angle is 44.1°, while the oil contact angle equals 135.9°. As

Table 1. Parameters Used in Simulations

parameters	OMP		
	92%	76%	50%
bulk oil−CO_2 viscosity/mPa·s	0.434	0.378	0.180
near-wall oil−CO_2 viscosity/mPa·s	0.700	0.750	0.800
near-wall thickness/nm	0.45	0.45	0.25
water contact angle/°	68.5	94.4	119.7
oil−CO_2 contact angle/°	111.5	85.6	60.3
G_{cs}, lu	−0.33	−0.28	−0.16
G_{os}, lu	−0.07	0.03	0.12

OMP decreases, the CO_2 mass content in oil−CO_2 miscible phase increases, and the water/oil−CO_2 miscible phase contact angle with $G_{cs} = -0.05$ increases/decreases. The fitting parameters of OMP equal to 92, 76, and 50% used in following flow simulations are given in Table 1.

$$k_{rw}(S_w) = \frac{\int_{|y|=0}^{w} u_w \mathrm{d}y}{\int_{|y|=0}^{t} u_w \mathrm{d}y} \tag{6}$$

$$k_{ro}(S_w) = \frac{\int_{|y|=0}^{o} u_{oc}\rho_o \mathrm{d}y}{\int_{|y|=0}^{t} u_{oc}\rho_o \mathrm{d}y} \tag{7}$$

Figures 13 and 14 present the oil−water relative permeability and distributions versus OMP. As OMP decreases, the oil relative permeability decreases, while the water relative permeability increases. It is because the increasing CO_2 content results in an increasing water contact angle. When OMP = 92%, there is some irreducible water, mainly in the form of a film existing on the pore wall or in the geometry corner because of the strong water-wetting. In addition, due to the water-wetting effect of the solid surface under the small CO_2 mass content, the distribution of the oil−

https://doi.org/10.1021/acs.langmuir.3c01570
Langmuir 2023, 39, 12226−12234

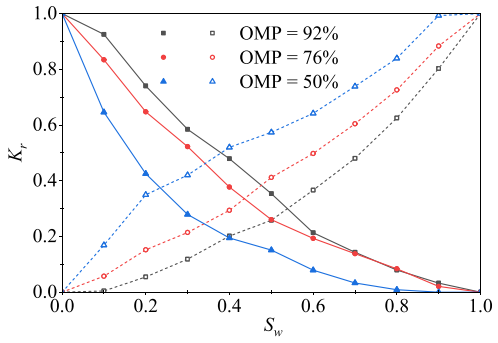

Figure 13. Relative permeability with different OMPs.

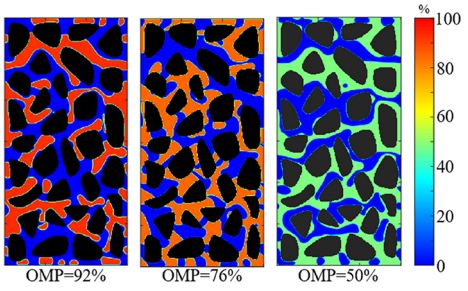

Figure 14. Oil−CO_2_water distributions with different OMPs and S_w = 0.5.

CO_2 miscible system is relatively dispersed. As OMP decreases, the water contact angle increases, and the small amount of water gradually changes from being a film to droplets and flows in the porous media. Moreover, the distribution of the oil−CO_2 miscible system changes from being dispersive to continuous. The irreducible water saturation approaches 0 in the ideal porous media used in this study.

CONCLUSIONS

In this work, an improved MCMP-LBM is proposed to investigate the effects of water phase on CO_2 sequestration during the CO_2 huff-n-puff process, and the effects of oil−CO_2 miscibility on oil−water flow behaviors and relative permeability are also studied. The interfacial tension and effects of oil−CO_2 miscibility on the water contact angle are successfully verified through the Laplace test and contact angle, respectively.

The results show that with a decrease of G_{cs} resulting in an increase in CO_2 adsorption capacity, CO_2 readily diffuses into the oil phase along the pore wall, and the CO_2 storage mass increases gradually. Additionally, in water-wetting porous media, water adsorbed on the pore surface gradually detaches from the wall and forms droplets due to the altered water contact angle by CO_2. In oil-wetting porous media, a small amount of water droplets can overcome Jamin's effect and are displaced out from the porous media. Due to Jamin's effect of water droplets in the oil-wetting pores and the capillary resistance of bridge-like water phase in water-wetting pores, CO_2 cannot diffuse into the oil phase, causing a large amount of oil confined in porous media. As water saturation increases, Jamin's effect and the capillary resistance of bridge-like water phase become more pronounced. In addition, the water phase occupies more pore space, and the solubility of CO_2 in water is negligible. As a result, the CO_2 storage mass gradually decreases.

By fitting the oil−CO_2 velocity and density distributions in calcite nanopores from MD simulations, the microscopic parameters for oil−CO_2−water three-component and two-phase flow simulations in calcite porous media are obtained. The results demonstrate that as OMP decreases, the oil/water relative permeability decreases/increases. In addition, the irreducible water content decreases. It is because the increasing CO_2 content results in an increasing water contact angle.

The porous media used in this work is conceptual and two-dimensional. Therefore, all discussions are qualitative analyses rather than quantitative calculations. Without considering high computing resources, the proposed model can be extended to simulate three-dimensional systems to accurately calculate the CO_2 geological storage mass considering the water saturation and relative permeability.

AUTHOR INFORMATION

Corresponding Authors

Jianchao Cai − *National Key Laboratory of Petroleum Resources and Engineering, China University of Petroleum, Beijing 102249, P. R. China;* orcid.org/0000-0003-2950-888X; Email: caijc@cup.edu.cn

Zhehui Jin − *School of Mining and Petroleum Engineering, Department of Civil and Environmental Engineering, University of Alberta, Edmonton, AB T6G 1H9, Canada;* orcid.org/0000-0001-8305-5637; Email: zhehui2@ualberta.ca

Authors

Han Wang − *National Key Laboratory of Petroleum Resources and Engineering, China University of Petroleum, Beijing 102249, P. R. China;* orcid.org/0009-0006-6827-0367

Yuliang Su − *Key Laboratory of Unconventional Oil & Gas Development (China University of Petroleum (East China)), Ministry of Education, Qingdao 266580, P. R. China; School of Petroleum Engineering, China University of Petroleum (East China), Qingdao 266580, P. R. China;* orcid.org/0000-0002-5977-4807

Mingshan Zhang − *Key Laboratory of Ministry of Education on Safe Mining of Deep Metal Mines, School of Resources and Civil Engineering, Northeastern University, Shenyang 110819, P. R. China*

Wendong Wang − *Key Laboratory of Unconventional Oil & Gas Development (China University of Petroleum (East China)), Ministry of Education, Qingdao 266580, P. R. China; School of Petroleum Engineering, China University of Petroleum (East China), Qingdao 266580, P. R. China;* orcid.org/0000-0001-9104-1622

Guanqun Li − *Key Laboratory of Unconventional Oil & Gas Development (China University of Petroleum (East China)), Ministry of Education, Qingdao 266580, P. R. China; School of Petroleum Engineering, China University of Petroleum (East China), Qingdao 266580, P. R. China*

Complete contact information is available at: https://pubs.acs.org/10.1021/acs.langmuir.3c01570

Notes

The authors declare no competing financial interest.

ACKNOWLEDGMENTS

This study was supported by the National Natural Science Foundation of China (42172159 and 51974348), a Discovery Grant from Natural Sciences and Engineering Research

Council of Canada (NSERC RGPIN-2017-05080), and China Postdoctoral Science Foundation (2023M733872).

REFERENCES

(1) Guan, Q.; Dong, D.; Wang, S.; Huang, J.; Wang, Y.; Lu, H.; Zhang, C. Preliminary study on shale gas microreservoir characteristics of the Lower Silurian Longmaxi Formation in the southern Sichuan Basin, China. *J. Nat. Gas. Sci. Eng.* **2016**, *31*, 382−395.
(2) Li, J.; Li, X.; Wu, K.; Feng, D.; Zhang, T.; Zhang, Y. Thickness and stability of water film confined inside nanoslits and nanocapillaries of shale and clay. *Int. J. Coal Geol.* **2017**, *179*, 253−268.
(3) Deng, H.; Sheng, G.; Zhao, H.; Meng, F.; Zhang, H.; Ma, J.; Gong, J.; Ruan, J. Integrated optimization of fracture parameters for subdivision cutting fractured horizontal wells in shale oil reservoirs. *J. Petrol. Sci. Eng.* **2022**, *212*, No. 110205.
(4) Siddhamshetty, P.; Wu, K.; Kwon, J. S.-I. Modeling and control of proppant distribution of multistage hydraulic fracturing in horizontal shale wells. *Ind. Eng. Chem. Res.* **2019**, *58* (8), 3159−3169.
(5) Feng, Q.; Xu, S.; Xing, X.; Zhang, W.; Wang, S. Advances and challenges in shale oil development: A critical review. *Adv. Geo-Energy Res.* **2020**, *4* (4), 406−418.
(6) Tu, J.; Sheng, J. J. Effect of pressure on imbibition in shale oil reservoirs with wettability considered. *Energy Fuels* **2020**, *34* (4), 4260−4272.
(7) Xu, G.; Han, Y.; Jiang, Y.; Shi, Y.; Wang, M.; Zeng, X. Reducing residual oil saturation: Underlying mechanism of imbibition in oil recovery enhancement of tight reservoir. *SPE J.* **2021**, *26*, 2340−2351, DOI: 10.2118/205491-PA.
(8) Wijaya, N.; Sheng, J. Effects of Imbibition During Well Shut-In on Ultimate Shale Oil Recovery: A Numerical Study. In *Paper presented at the SPE Western Regional Meeting, Virtual*, April **2021**, SPE200875.
(9) Akbarabadi, M.; Saraji, S.; Piri, M.; Georgi, D.; Delshad, M. Nano-scale experimental investigation of in-situ wettability and spontaneous imbibition in ultra-tight reservoir rocks. *Adv. Water Resour.* **2017**, *107*, 160−179.
(10) Siddiqui, M. A. Q.; Chen, X.; Iglauer, S.; Roshan, H. A multiscale study on shale wettability: Spontaneous imbibition versus contact angle. *Water Resour. Res.* **2019**, *55* (6), 5012−5032.
(11) Birdsell, D. T.; Rajaram, H.; Lackey, G. Imbibition of hydraulic fracturing fluids into partially saturated shale. *Water Resour. Res.* **2015**, *51* (8), 6787−6796.
(12) Li, C.; Singh, H.; Cai, J. Spontaneous imbibition in shale: A review of recent advances. *Capillarity* **2019**, *2* (2), 17−32.
(13) Wang, H.; Wang, W.; Su, Y.; Jin, Z. Lattice Boltzmann model for oil/water two-phase flow in nanoporous media considering heterogeneous viscosity, liquid/solid, and liquid/liquid Slip. *SPE J.* **2022**, *27*, 3508−3524.
(14) Wang, H.; Su, Y.; Wang, W.; Li, L.; Sheng, G.; Zhan, S. Relative permeability model of oil-water flow in nanoporous media considering multi-mechanisms. *J. Petrol. Sci. Eng.* **2019**, *183*, No. 106361.
(15) Zhang, W.; Feng, Q.; Jin, Z.; Xing, X.; Wang, S. Molecular simulation study of oil-water two-phase fluid transport in shale inorganic nanopores. *Chem. Eng. Sci.* **2021**, *245*, No. 116948.
(16) Syed, F. I.; Muther, T.; Van, V. P.; Dahaghi, A. K.; Negahban, S. Numerical trend analysis for factors affecting EOR performance and CO_2 storage in tight oil reservoirs. *Fuel* **2022**, *316*, No. 123370.
(17) Sambo, C.; Liu, N.; Shaibu, R.; Ahmed, A. A.; Hashish, R. G. A technical review of CO_2 for enhanced oil recovery in unconventional oil reservoirs. *J. Petrol. Sci. Eng.* **2023**, *221*, 111185.
(18) Qin, X.; Singh, H.; Cai, J. Sorption characteristics in coal and shale: A review for enhanced methane recovery. *Capillarity* **2022**, *5* (1), 1−11.
(19) Kumar, N.; Sampaio, M. A.; Ojha, K.; Hoteit, H.; Mandal, A. Fundamental aspects, mechanisms and emerging possibilities of CO_2 miscible flooding in enhanced oil recovery: A review. *Fuel* **2022**, *330*, No. 125633.
(20) Guo, H.; Wang, Z.; Wang, B.; Zhang, Y.; Meng, H.; Sui, H. Molecular dynamics simulations of oil recovery from dolomite slit nanopores enhanced by CO_2 and N_2 injection. *Adv. Geo-Energy. Res.* **2022**, *6* (4), 306−313.
(21) Moh, D. Y.; Zhang, H.; Wang, S.; Yin, X.; Qiao, R. Soaking in CO_2 huff-n-puff: A single-nanopore scale study. *Fuel* **2022**, *308*, No. 122026.
(22) Zhang, W.; Feng, Q.; Wang, S.; Xing, X.; Jin, Z. CO_2-regulated octane flow in calcite nanopores from molecular perspectives. *Fuel* **2021**, *286*, No. 119299.
(23) Li, W.; Zhang, M.; Nan, Y.; Pang, W.; Jin, Z. Molecular dynamics study on CO_2 storage in water-filled kerogen nanopores in shale reservoirs: Effects of kerogen maturity and pore size. *Langmuir* **2021**, *37* (1), 542−552.
(24) Zhang, M.; Zhan, S.; Jin, Z. Recovery mechanisms of hydrocarbon mixtures in organic and inorganic nanopores during pressure drawdown and CO_2 injection from molecular perspectives. *Chem. Eng. J.* **2020**, *382*, No. 122808.
(25) Zhang, X.; Su, Y.; Li, L.; Hao, Y.; Wang, W.; Liu, J.; Gao, X.; Zhao, A.; Wang, K. Microscopic remaining oil initiation mechanism and formation damage of CO_2 injection after waterflooding in deep reservoirs. *Energy* **2022**, *248*, No. 123649.
(26) Xiong, H.; Devegowda, D.; Huang, L. Water bridges in clay nanopores: mechanisms of formation and impact on hydrocarbon transport. *Langmuir* **2020**, *36* (3), 723−733.
(27) Kim, C.; Devegowda, D. Molecular dynamics study of fluid-fluid and solid-fluid interactions in mixed-wet shale pores. *Fuel* **2022**, *319*, No. 123587.
(28) Cai, J.; Jin, T.; Kou, J.; Zou, S.; Xiao, J.; Meng, Q. Lucas−Washburn equation-based modeling of capillary-driven flow in porous systems. *Langmuir* **2021**, *37* (5), 1623−1636.
(29) Liu, B.; Liu, W.; Pan, Z.; Yu, L.; Xie, Z.; Lv, G.; Zhao, P.; Chen, D.; Fang, W. Supercritical CO_2 breaking through a water bridge and enhancing shale oil recovery: A molecular dynamics simulation study. *Energy Fuels* **2022**, *36* (14), 7558−7568.
(30) Luan, Y.; Dou, X.; Zhou, Y.; Hao, P.; Liu, B.; Liu, J. Effect of the water film rupture on the oil displacement by supercritical CO_2 in the nanopore: Molecular dynamics simulations. *Energy Fuels* **2022**, *36* (8), 4348−4357.
(31) Yong, W.; Derksen, J.; Zhou, Y. The influence of CO_2 and CH_4 mixture on water wettability in organic rich shale nanopore. *J. Nat. Gas Sci. Eng.* **2021**, *87*, No. 103746.
(32) Zhou, J.; Zhang, J.; Yang, J.; Jin, Z.; Luo, K. H. Mechanisms for kerogen wettability transition from water-wet to CO_2-wet: Implications for CO_2 sequestration. *Chem. Eng. J.* **2022**, *428*, No. 132020.
(33) Sun, S.; Liang, S.; Liu, Y.; Liu, D.; Gao, M.; Tian, Y.; Wang, J. A review on shale oil and gas characteristics and molecular dynamics simulation for the fluid behavior in shale pore. *J. Mol. Liq.* **2023**, *376*, No. 121507.
(34) Li, L.; Sheng, J. J.; Su, Y.; Zhan, S. Further investigation of effects of injection pressure and imbibition water on CO2 huff-n-puff performance in liquid-rich shale reservoirs. *Energy Fuels* **2018**, *32* (5), 5789−5798.
(35) Jiang, F.; Tsuji, T. Estimation of three-phase relative permeability by simulating fluid dynamics directly on rock-microstructure images. *Water Resour. Res.* **2017**, *53* (1), 11−32.
(36) Ashirbekov, A.; Kabdenova, B.; Kuljabekov, A.; Monaco, E.; Wang, L.; Rojas-Solórzano, L. Lattice Boltzmann pseudopotential multiphase modeling of transcritical CO_2 flow using a crossover formulation. *Adv. Geo-Energy. Res.* **2022**, *6* (6), 539−540.
(37) Liu, Y.; Berg, S.; Ju, Y.; Wei, W.; Kou, J.; Cai, J. Systematic investigation of corner flow impact in forced imbibition. *Water Resour. Res.* **2022**, *58* (10), No. e2022WR032402.
(38) Liu, Y.; Zou, S.; He, Y.; Sun, S.; Ju, Y.; Meng, Q.; Cai, J. Influence of fractal surface roughness on multiphase flow behavior: Lattice Boltzmann simulation. *Int. J. Multiphase Flow.* **2021**, *134*, No. 103497.

https://doi.org/10.1021/acs.langmuir.3c01570
Langmuir 2023, 39, 12226−12234

(39) Zhao, J.; Liu, Y.; Qin, F.; Fei, L.; Wang, Y.; Shang, Q.; Guo, J.; Zhou, L. Pore-scale fluid flow simulation coupling lattice Boltzmann method and pore network model. *Capillarity* **2023**, *7* (3), 41−46.
(40) Wei, B.; Huang, H.; Hou, J.; Sukop, M. C. Study on the meniscus-induced motion of droplets and bubbles by a three-phase Lattice Boltzmann model. *Chem. Eng. Sci.* **2018**, *176*, 35−49.
(41) Zhu, X.; Wang, S.; Feng, Q.; Zhang, L.; Chen, L.; Tao, W. Pore-scale numerical prediction of three-phase relative permeability in porous media using the lattice Boltzmann method. *Int. Commun. Heat. Mass Trans.* **2021**, *126*, No. 105403.
(42) Li, S.; Lu, Y.; Jiang, F.; Liu, H. Lattice Boltzmann simulation of three-phase flows with moving contact lines on curved surfaces. *Phys. Rev. E* **2021**, *104* (1), No. 015310.
(43) Yu, Y.; Liang, D.; Liu, H. Lattice Boltzmann simulation of immiscible three-phase flows with contact-line dynamics. *Phys. Rev. E* **2019**, *99* (1), No. 013308.
(44) Tang, M.; Zhan, H.; Lu, S.; Ma, H.; Tan, H. Pore-scale CO_2 displacement simulation based on the three fluid phase lattice Boltzmann method. *Energy Fuels* **2019**, *33* (10), 10039−10055.
(45) Gao, J.; Xing, H.; Tian, Z.; Pearce, J. K.; Sedek, M.; Golding, S. D.; Rudolph, V. Reactive transport in porous media for CO_2 sequestration: Pore scale modeling using the lattice Boltzmann method. *Comp. Geosci.* **2017**, *98*, 9−20.
(46) Chen, Y.; Li, Y.; Valocchi, A. J.; Christensen, K. T. Lattice Boltzmann simulations of liquid CO_2 displacing water in a 2D heterogeneous micromodel at reservoir pressure conditions. *J. Contam. Hydrol.* **2018**, *212*, 14−27.
(47) Kohanpur, A. H.; Rahromostaqim, M.; Valocchi, A. J.; Sahimi, M. Two-phase flow of CO_2-brine in a heterogeneous sandstone: Characterization of the rock and comparison of the lattice-Boltzmann, pore-network, and direct numerical simulation methods. *Adv. Water Resour.* **2020**, *135*, No. 103469.
(48) An, S.; Erfani, H.; Hellevang, H.; Niasar, V. Lattice-Boltzmann simulation of dissolution of carbonate rock during CO_2-saturated brine injection. *Chem. Eng. J.* **2021**, *408*, No. 127235.
(49) Wang, H.; Su, Y.; Wang, W.; Jin, Z.; Chen, H. CO_2-oil diffusion, adsorption and miscible flow in nanoporous media from pore-scale perspectives. *Chem. Eng. J.* **2022**, *450*, No. 137957.
(50) Benzi, R.; Biferale, L.; Sbragaglia, M.; Succi, S.; Toschi, F. Mesoscopic modeling of a two-phase flow in the presence of boundaries: the contact angle. *Phys. Rev. E* **2006**, *74* (2), No. 021509.
(51) Zhang, T.; Javadpour, F.; Li, X.; Wu, K.; Li, J.; Yin, Y. Mesoscopic method to study water flow in nanochannels with different wettability. *Phys. Rev. E* **2020**, *102* (1), No. 013306.
(52) Feng, D.; Li, X.; Wang, X.; Li, J.; Zhang, T.; Sun, Z.; He, M.; Liu, Q.; Qin, J.; Han, S. Capillary filling of confined water in nanopores: coupling the increased viscosity and slippage. *Chem. Eng. Sci.* **2018**, *186*, 228−239.
(53) Saraji, S.; Piri, M.; Goual, L. The effects of SO_2 contamination, brine salinity, pressure, and temperature on dynamic contact angles and interfacial tension of supercritical CO_2/brine/quartz systems. *Int. J. Greenhouse Gas. Control.* **2014**, *28*, 147−155.
(54) Xing, W.; Song, Y.; Zhang, Y.; Nishio, M.; Zhan, Y.; Jian, W.; Shen, Y. Research progress of the interfacial tension in supercritical CO2-water/oil system. *Energy Procedia* **2013**, *37*, 6928−6935.
(55) Zhao, L.; Lin, S.; Mendenhall, J. D.; Yuet, P. K.; Blankschtein, D. Molecular dynamics investigation of the various atomic force contributions to the interfacial tension at the supercritical CO_2−water interface. *J. Phys. Chem. B* **2011**, *115* (19), 6076−6087.
(56) Georgiadis, A.; Maitland, G.; Trusler, J. M.; Bismarck, A. Interfacial tension measurements of the (H2O+ CO2) system at elevated pressures and temperatures. *J. Chem. Eng. Data* **2010**, *55* (10), 4168−4175.
(57) Bikkina, P. K.; Shoham, O.; Uppaluri, R. Equilibrated interfacial tension data of the CO_2−water system at high pressures and moderate temperatures. *J. Chem. Eng. Data* **2011**, *56* (10), 3725−3733.
(58) Yekeen, N.; Padmanabhan, E.; Idris, A. K. Synergistic effects of nanoparticles and surfactants on n-decane-water interfacial tension and bulk foam stability at high temperature. *J. Petrol. Sci. Eng.* **2019**, *179*, 814−830.
(59) Arabloo, M.; Ghazanfari, M. H.; Rashtchian, D. Wettability modification, interfacial tension and adsorption characteristics of a new surfactant: Implications for enhanced oil recovery. *Fuel* **2016**, *185*, 199−210.
(60) Li, C.; Li, Y.; Pu, H. Molecular simulation study of interfacial tension reduction and oil detachment in nanochannels by Surface-modified silica nanoparticles. *Fuel* **2021**, *292*, No. 120318.
(61) Wang, F.; Zhao, J. Mathematical modeling of gravity and buoyancy effect on low interfacial tension spontaneous imbibition in tight oil reservoirs. *AlChE J.* **2021**, *67* (9), No. e17332.
(62) Sukee, A.; Nunta, T.; Haruna, M. A.; Kalantariasl, A.; Tangparitkul, S. Influence of sequential changes in the crude oil-water interfacial tension on spontaneous imbibition in oil-wet sandstone. *J. Petrol. Sci. Eng.* **2022**, *210*, No. 110032.
(63) Hassan, M.; Nielsen, R.; Calhoun, J. Effect of pressure and temperature on oil-water interfacial tensions for a series of hydrocarbons. *J. Petrol. Technol.* **1953**, *5* (12), 299−306.
(64) Liu, B.; Shi, J.; Wang, M.; Zhang, J.; Sun, B.; Shen, Y.; Sun, X. Reduction in interfacial tension of water−oil interface by supercritical CO_2 in enhanced oil recovery processes studied with molecular dynamics simulation. *J. Super. Fluids* **2016**, *111*, 171−178.
(65) Zhang, T.; Javadpour, F.; Li, J.; Zhao, Y.; Zhang, L.; Li, X. Pore-scale perspective of gas/water two-phase flow in shale. *SPE J.* **2021**, *26* (02), 828−846.
(66) Wei, B.; Hou, J.; Sukop, M. C.; Du, Q. Enhancing oil recovery using an immiscible slug: Lattice Boltzmann simulation by three-phase pseudopotential model. *Phys. Fluids* **2020**, *32* (9), No. 092105.
(67) Yiotis, A. G.; Psihogios, J.; Kainourgiakis, M. E.; Papaioannou, A.; Stubos, A. K. A lattice Boltzmann study of viscous coupling effects in immiscible two-phase flow in porous media. *Colloid Surf. A: Physicochem. Eng. Asp.* **2007**, *300* (1−2), 35−49.
(68) Wijaya, N.; Sheng, J. J. Uncertainty quantification of shale capillary desaturation curves for surfactant EOR in shale through fracturing fluids using predictive modeling. *Fuel* **2021**, *283*, No. 118857.
(69) Qin, C.; Jiang, Y.; Zhou, J.; Zuo, S.; Chen, S.; Liu, Z.; Yin, H.; Li, Y. Influence of supercritical CO_2 exposure on water wettability of shale: Implications for CO_2 sequestration and shale gas recovery. *Energy* **2022**, *242*, 122551.
(70) Samara, H.; Ke, L.; Ostrowski, T.; Ganzer, L.; Jaeger, P. Unconventional oil recovery from Al Sultani tight rock formations using supercritical CO_2. *J. Super. Fluids* **2019**, *152*, No. 104562.
(71) Wu, K.; Chen, Z.; Li, J.; Li, X.; Xu, J.; Dong, X. Wettability effect on nanoconfined water flow. *Proc. Nat. Acad. Sci. U. S. A.* **2017**, *114* (13), 3358−3363.

https://doi.org/10.1021/acs.langmuir.3c01570
Langmuir 2023, 39, 12226−12234